ELSEVIER

International Journal of Mass Spectrometry 213 (2002) 203–215

www.elsevier.com/locate/ijms

Delayed extraction experiments using a repulsive potential before ion extraction: Evidence of clusters as ion precursors in UV-MALDI. Part I: Dynamical effects with the matrix 2,5-dihydroxybenzoic acid

I. Fournier, A. Brunot, J.C. Tabet, G. Bolbach*

Université P & M CURIE,Laboratoire de Chimie Structurale Organique et Biologique, CNRS-UMR7613, Boîte 45, 4 Place Jussieu 75252 Paris Cedex05, France

Received 26 July 2001; accepted 1 October 2001

Abstract

Delayed extraction experiments were undertaken to precise the dynamical effects involved in the ion formation in ultraviolet matrix-assisted laser desorption/ionization (UV-MALDI). Careful examination of the ion time-of-flight variation with the extraction delay time were performed with a repulsive potential before ion extraction. Depending on the mass of the ion (matrix 2,5-dihydroxybenzoic acid and peptides) and on the repulsing potential, some deviations from the linear relationship between the ion time-of-flight and the delay time were observed. Simulations of the ion time-of-flight clearly show that ions are not directly produced on the target surface but originate from the gas-phase decomposition of higher mass precursors. The size of the precursor, composed of the analyte surrounded by matrix molecules, increases with that of the analyte. Complete desolvation of the cluster-precursor could be likely induced by the high electric field transient during the pulse extraction. The existence of clusters as precursor of the ion production in MALDI highlights a new global frame to explain the analyte protonation in UV-MALDI. (Int J Mass Spectrom 213 (2002) 203–215) © 2002 Elsevier Science B.V.

Keywords: MALDI; Time-of-flight mass spectrometry; Ablation; Ion formation: Mechanisms

1. Introduction

The high performance of matrix-assisted laser desorption/ionization (MALDI) coupled to time-of-flight (TOF) mass spectrometry is now well recognized especially for the characterization of biomolecules such as proteins, oligosaccharides and DNA. In particular, MALDI-TOFMS is a powerful tool for the proteomic applications. Despite the widespread analytical applications, the ion production mechanisms involved in MALDI are still rather poorly understood. Similar comments can also be applied for the precise details of ion production by electrospray. These two ionization methods, appearing complementary for applications, give a new example of what was previously written by Ligon and Dorn [1] about the secondary ion mass spectrometry (SIMS) of liquid surfaces: " . . .you do not always need to know what you are doing to get useful information". The main

* Corresponding author. E-mail: bolbach@ccr.jussieu.fr

PII S1387-3806(01)00540-1

difficulties to understand the mechanisms of ion production induced by particle impact (photons, ions..) are due to the time and space scales on which these mechanisms occur, i.e < a few ns and ~nm on the surface or in the selvedge, compared to those scales for which the information on the ions is obtained, i.e ~a few μs to a few tens of μs and ~1 m (detector). All things considered, the situation is similar to study the big bang (ion formation) from the observation of the universe at present time (ion detection).

In MALDI, some information has been gained from the relaxation processes of the absorbed photon in solid state. Studies of the luminescence emission after the laser shot [2–4] is the only way to get a direct observation of what happens on the target in the few ns after the beam impact through photon emission from electronically excited states of matrix molecules. Briefly, it has been shown that fluorescence emission, with lifetime <1 ns for the most common matrices [2,3], is partly quenched when the laser fluence achieves the threshold for ion production [2]. This indicates that the ion production is connected to an internal energy conversion in the solid state through the so-called energy pooling [4] likely resulting from reactive collisions between excited singlet states [3]. The energy pooling model, including photothermal/ionization [5] and multi-center excitation, was developed to take into account that ion production cannot be induced by direct photoionization of the matrix molecules [4]. Storage energy mechanisms have also been shown to be operative in MALDI as pointed out by the experiments using two time-delayed laser pulses for which the maximum matrix ion production is achieved for an optimal time delay between the two laser shots [6,7]. In this experiment, two regimes were found for the 2,5-DHB matrix, a fast one with the two laser beams bombarding the target within very short delay time (0.1 ns), and a slower one corresponding to a higher delay time (~ 2 ns) and a stronger ion production. There is no direct proof that the slowest regime involves molecules in the gas phase when the fastest regime involves molecules in the condensed phase.

Basically, in a MALDI experiment, the separation between ablation (more appropriate than the usually employed “desorption”) and ionization events is not straightforward since the only information on the ion are obtained by the mass spectrometer through the ion time-of-flight, as above mentioned, very far from the surface target and its “selvedge” and at relatively long time after the start of ablation step.

The ablation leads to the so-called plume as shown by modeling the ejection process [8,9]. Real imaging of the plume and its temporal progression using laser-induced fluorescence were reported in MALDI experiment for 3-hydroxypicolinic acid matrix [10]. The resulting images present a dense plume mainly composed of intact matrix molecules and a minor component of ions (four orders of magnitude lower) compared to neutrals. In addition, the initial plume velocity is superthermal (~1 000 m/s) [10]. The initial axial velocity, in particular for ions, was also extensively studied [11–16] and it lies in the 300–1500 m/s range, but there is still a large scattering in the measured values for a given matrix and analyte. This scattering can originate from sample preparation, nature and chemical properties of both the matrix and analyte [16] but also from the methods and approximations used to extract and/or calculate the initial velocity. Although the initial radial velocity was not so deeply investigated, its value seems to be smaller than the axial one [17,18] in good agreement with the picture of matter ejection as a supersonic beam. Other experiments were reported on the ion kinetic energy deficit in continuous ion extraction [17] and interpreted as the result of collisions between ions and the dense neutral material in the plume.

The chemical aspects of the UV/MALDI ionization processes are also not yet really understood and the question of how and where the analyte ions are formed is still open. However, some reasonable attempts were published to explain some particular cases [19] or to extract a more general and rational frame [20].

The aim of the presented work was to study the dynamical aspects of the ion production and search for the existence of precursors for the different ions (matrix and analytes) in the early stages of the plume expansion. If such precursors do exist, the ion time-

of-flight must contain the "history" of the ion formation from the precursors to the expected ions, even if these precursors will weakly contribute to the ion time-of-flight. Thus, delayed extraction is a method of choice for such a purpose since, in principle it allows a natural evolution of the plume in a controlled time range (delay time) and in controlled manner (no or weak electric field). The time-of-flight of various ions was systematically studied as a function of the ion *m/z* ratio and the delayed extraction conditions i.e. the delay time and repulsing field in the first extraction region before the ion extraction step.

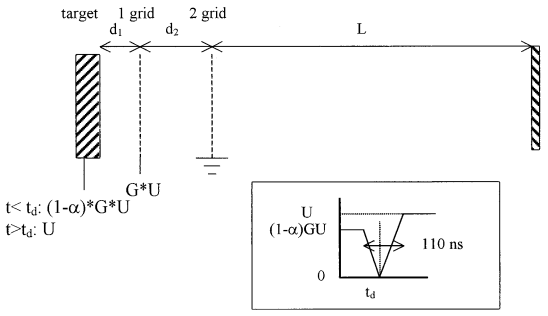

Fig. 1. Schematic diagram of the linear TOF mass spectrometer showing the voltage applied to the target in the delayed extraction mode. The inset shows the variation of target voltage during the voltage switch associated to the ion extraction.

2. Experimental

2.1. Target preparation

For these experiments the dried-droplet standard preparation was used by depositing 1 μl of 2,5-dihydroxybenzoic acid (Aldrich) solution (9×10^{-2} M in ACN:H_2O 4:1 v:v) containing peptide mixture (substance P mw=1 347.6, ACTH 18-39 mw=2 465.7, ACTH 7-38 mw=3 659.2, and bovine insulin mw=5 733.6, all from Sigma, and dissolved in water) on the target holder (100 position gold coated plate). The molar ratio peptide/matrix was in the range 1/10 000–1/100 000. All the experiments were performed on the same sample holder and at the same position in order to reduce the possible variation of the distance in the first extraction region.

2.2. Delayed extraction

Experiments on the variation of the matrix and peptide ion time-of-flight versus the delay time were performed on a Voyager Elite TOF mass spectrometer (PE Biosystems, Framingham, MA, USA) in the linear mode. This instrument is equipped with a nitrogen laser (Laser Science, Franklin, MA, USA) emitting at 337 nm and focalized onto the target with an angle of incidence of 45°. Ion focalization along the drift tube is achieved by an ion wire guide. The laser energy was chosen to be 1.2 times the threshold energy for the peptide ion production (signal/noise ~2). The detector provided by the constructor is a prototype for high *m/z* ion detection including a microchannel plate (ion-electron conversion), a scintillator (electron-photon conversion), a light condenser and a photo multiplier. The ion signal was digitized at a rate of 500 MHz by a Tektronix TD520 digitizing oscilloscope (2 ns resolution). Typically 128 to 256 mass spectra were averaged on various spots of the target. Mass spectra were analyzed using the GRAMS/386 software (Galactic).

Careful examination of the delayed extraction (DE) including both geometrical distances of the extracting stages and high voltage switch were operated. In the instrument, the ion extraction region is composed of two stages (Fig. 1). The distance d_1 from the target to the first grid (90% transmission Ni mesh) was determined ($d_1=3.55\pm0.05$ mm). The distance d_2 from the first to the second grid (90% transmission) is 18.0 mm. The drift tube length L indicated by the constructor is 1.9335 m. These measurements were verified by studying the matrix and peptide ion time-of-flight in the continuous linear extraction mode in which the target was held to potential U, the first grid to G*U (the parameter G varying from 0.90 to 0.60) and the second grid is grounded. In this mode, the dynamical effects of ablation/ion formation are negligible and calculation of the time-of-flight can be compared to experimental values taking into account the signal propagation times in the wires. Using 2,5 DHB target doped with the four analytes above

mentioned, the best fit was obtained for $d_1=3.55\pm0.05$ mm, $d_2=18.1$ mm, $L=1.93$ m and an initial axial velocity $v_0=850\pm200$ m/s.

In the DE mode, the field penetration of the second extracting stage into the first has to be taken into account. In the instrument, to compensate partly this effect, the target voltage is held to a potential of (1-α)*G*U before the application of the ion extraction pulse and it is switched to U after the extraction pulse (Fig. 1). In this operation two different HV power supplies are used, allowing to switch the target voltage. The first grid voltage remains at G*U (the parameter $G < 1$ is controlled through the computer). It was experimentally determined that $\alpha=0.0011$. The total duration of the HV switch was measured to be ~110 ns using low U voltage. During this pulse, the target voltage decreased from (1-α)*G*U to a much lower value near the ground (in ~30 ns) and then increased up to U (in ~80 ns). It should be noted that during the extraction pulse switch the variations of the electric field in the first stage are extremely strong ($\Delta E \sim 2U/d_1$). Such variations could account for the ion formation as discussed below. The TOF start signal is triggered by the electronics of the delayed extraction and not directly by the laser pulse. The dead time for the DE electronics was measured to 200 ns, thus the shorter delay time in these experiments was fixed to 200 ns. Taking into account the signal propagation time (start and stop) and the delay of the electronics, the measured time-of-flight, tof(pulse), triggered by the extraction pulse was converted in time-of-flight, tof(laser), triggered by the laser shot as a function of the delay time t_d: tof(laser) = tof(pulse) $+t_d$ +85 ns.

2.3. Study of the potential distribution in the first stage of the extraction region prior ion extraction

In its principle, delayed extraction implies that the matter ejected from the surface evolves in a totally field free region and moves with its own initial velocity distribution before ion extraction step. Any stray field (field penetration through grids, fringing field, dielectric effects. . ..) will cause that the first stage is not really field free. In our experiments, the ion signal disappearance observed for the lightest ions (typically matrix ions) and for the longest delay times (see results) gave evidence that such stray fields could play a role to modify the ion trajectory during the delay time period. This artifact, if ignored, could also lead to a false interpretation of the ion formation dynamic.

The potential distribution in the first extraction stage was simulated with SIMION software (V6.0) [21] considering the potential applied on the target and the grids before ion extraction and the geometry (d_1 and d_2 experimentally determined) of the extraction region. The simulation was carried out with the maximum resolution allowable by the software (10^7 points). The first grid was simulated by 25 meshes using the grid geometry (wire diameter and spacing distance) as measured with an optical microscope. The second stage was simulated only up to 6.8 mm ($d_2=18$ mm) to keep the maximum resolution. The potential distribution was determined for various conditions ($d_1=3.6$, 3.3, and 2.9 mm, $d_2=18$ mm, U= 15, 20, 25 kV, G=0.90, 0.92, 0.94, and 0.96 with $\alpha=0.0011$). No radial voltage gradient was found excepted at short distances from the grid (<0.2 mm).

As expected, the potential distribution strongly depends upon the d_1 distance (Fig. 2a). For $d_1=2.9$ mm, the potential slowly decreases as a function of the distance to the target indicating that ions are weakly accelerated (8 V over 1 mm) during the delay time. In our specific experimental conditions ($d_1=3.6$ mm), the potential strongly increases of ~40 V up to a distance of 1.5 mm from the target. It remains constant from 1.5 to 2 mm and decreases beyond. Thus, the potential is repulsing near the target surface and ions can be slowed down when they left the target surface. For the lightest ions, which have a low initial kinetic energy, this repulsing potential distribution can account for the absence of ion detection due to a come back of these ions to the target (see discussion below). As shown in Fig. 2b, the potential distribution is proportional to G and U indicating that in our experiment the repulsing field can be controlled prior to ion extraction step. It was assumed that the constant time-of-flight of Na^+ and K^+ ions as a function of the delay time is a proof of the non-existence of such

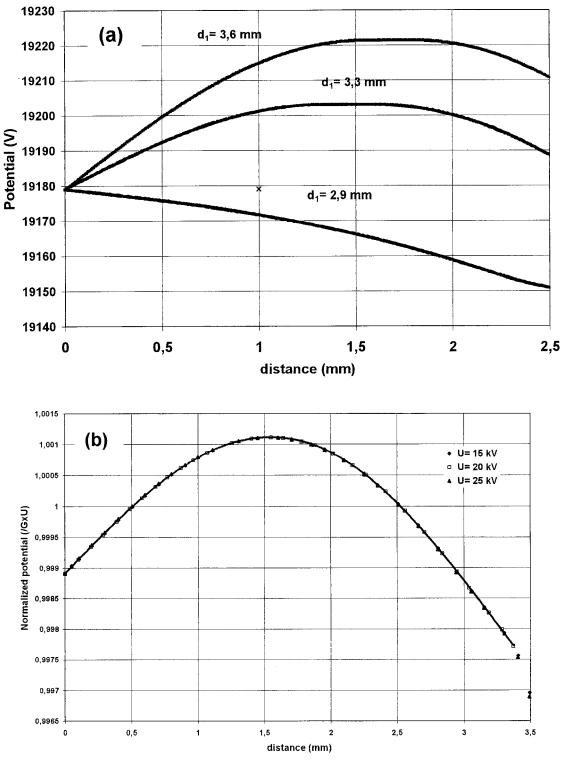

Fig. 2. Potential distribution in the first acceleration stage prior to the delayed extraction pulse as determined by simulations using SIMION (see text), (a) for different length d_1 of the stage with U=20 kV, G=0.96 and $\alpha = -0.0011$ and (b) normalized potential distribution for different U (15, 20, and 25 kV) and G (0.90–0.96) values (d_1=3.6 mm).

fields [15,16]. In our opinion this is not sufficient and another condition i.e., the constant ion intensity in the delay time range, must also be required. In our experiments, the time-of-flight of these ions are constant in the 200–1800 ns range but the intensity drastically dropped by more than two orders of magnitude; the ion intensity decay being more pronounced when the repulsion field increases.

3. Results

Systematic studies on the variation of ion time-of-flight (peak centroid, FWHM and intensity) with respect to the extraction delay time (200–2 200 ns and often extended to 3 200 ns) were carried out for different values of U and G and consequently for various repulsing potentials before the ion extraction step.

3.1. Ion time-of-flight centroid dependence upon extraction delay time

Fig. 3 shows typical examples of this variation for matrix and peptide ions (U=20 kV). On the same target and at the same area, the observed variations are quite reproducible for different deposits carried out at different delay times. The uncertainties on the tof measurements, indicated by the error bars in Fig. 3 were obtained for the same deposit.

The main feature observed from these curves is that the evolution is not completely linear in all the studied t_d range. The extension of linearity increases with the ion mass but it decreases when G and/or U increase(s). For instance, the tof variation for the mH^+ ions of the matrix is not linear though a pseudo-linearity could be assumed in the 300–600 ns range (Fig. 3e and 3f). For the MH^+ ion of substance P, the linearity is noted in the ranges 400–1300 ns and 400–2 000 ns respectively for U=25 kV, G=0.94 and U=15 kV, G=0.94 (data not shown). In addition, for U=20 kV, the extension of linearity is larger for G=0.9 than for G=0.96 (Fig. 3a and 3c). For the MH^+ ions of insulin the linearity is found in the t_d range 400–2 200 ns (Fig. 3b and 3d). Intermediate extensions were found for ACTH18-39 and ACTH 7-38 MH^+ ion. Systematic errors in the TOF measurements can be excluded since the data on matrix and peptide ions are analyzed from the same mass spectrum. These results give evidence that the repulsing potential in the first stage play a role in the ion time-of-flights. For peptide ions and for t_d <400 ns, tof values are systematically higher than the value expected from the extrapolation of the linear dependence. Careful measurements in the range 200–400 ns clearly confirmed this result.

3.2. Resolution and extraction delay time

The tof peak resolution defined as R=tof_c/(2xFWHM), where tof_c is the peak centroid and FWHM is

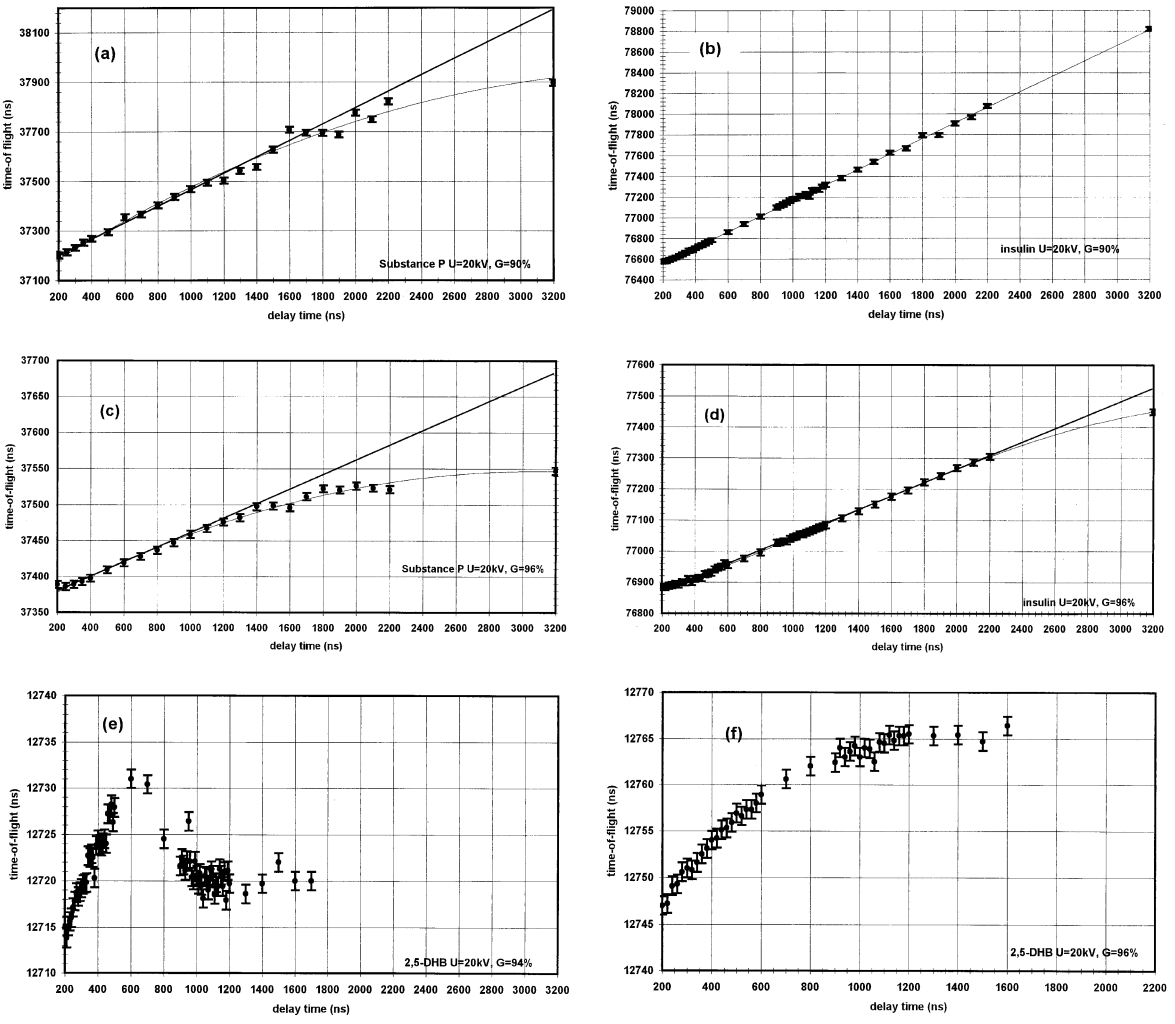

Fig. 3. Typical variation of the quasimolecular ion flight times as a function of the extraction delay time for U=20 kV: (a) substance P, G=0.90, (b) bovine insulin, G=0.90, (c) substance P, G=0.96, (d) bovine insulin, G=0.96, (e) 2,5-DHB, G=0.94, and (f) 2,5-DHB, G=0.96. The error bars correspond to the uncertainties obtained on various sets of experiments on a same target.

the peak full width at half maximum also strongly depend on the ion *m/z* ratio, voltage U and value of G. In particular, the delay time for which the resolution is maximum (R∼700 to 900) increases with the ion *m/z* ratio. Typically for U=20 kV and G=0.94, this delay time is respectively 325, 425, 465, and 595±40 ns for the protonated molecule of substance P, ACTH18-39, ACTH 7-38 and bovine insulin. It increases when decreasing U and increasing G. The influence of these parameters will be discussed below.

3.3. Ion intensity variation with the delay time

In spite of the scattering of the intensity values, mainly due to local target non homogeneity, general trends can be drawn. For the matrix mH^+ ion (Fig. 4c), the intensity increases with t_d up to ∼800 ns and decreases slightly beyond. The intensity drops to zero for increasing t_d values when G (or U) decreases respectively from 0.96 to 0.90 (or from 20 to 15 kV). When the voltage U was held to 25 kV, the signal

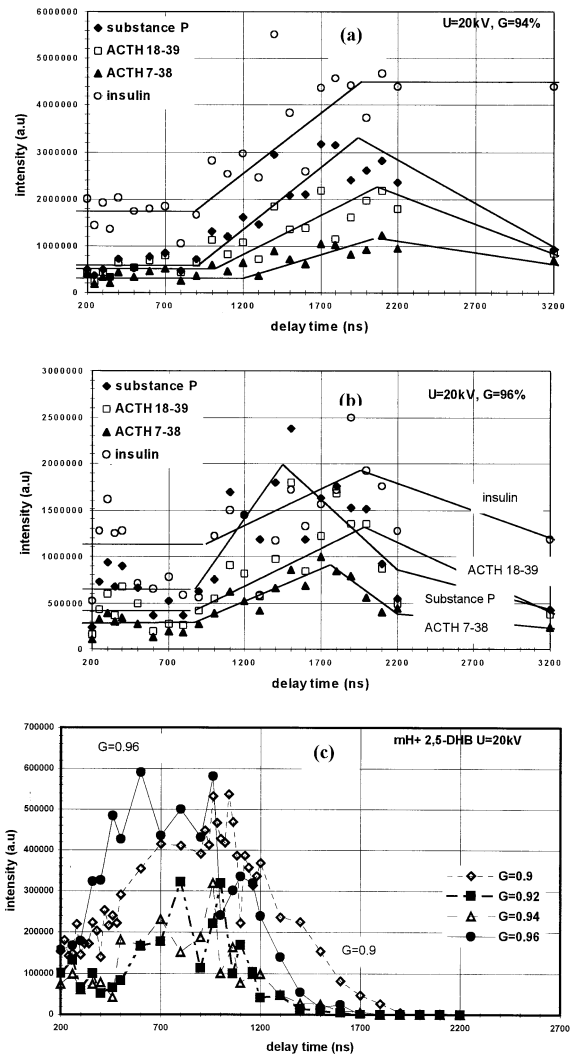

Fig. 4. Ion abundance as a function of the extraction delay time: for the protonated molecule of the peptides (SP: substance P, ACTH 18-39, ACTH 7-38 and bovine insulin) using U=20 kV (a) G=0.94 and (b) G=0.96, and (c) for the protonated molecule of the 2,5-DHB matrix with G=0.90, 0.92, 0.94, and 0.96 (see text). The lines in (a) and (b) are used as a eye guide to indicate the global evolution which is reproducible from one experiment to another.

disappears at shorter t_d (data not shown). The intensity of the peptide MH^+ ion remains constant up to t_d ~1 000 ns (Fig. 4a and 4b). For the higher t_d values two behaviors have to be noted. For the lowest G values (G=0.90), the intensity increases roughly linearly with t_d for all the peptides. However for the highest G values (G=0.96) and for the lighter peptides, such as substance P, the intensity first increases and then decreases. This clearly shows that ion abundance also depends upon the repulsing potential in the first stage. We should note that the initial radial velocity cannot be invoked to account for the ion signal disappearance at longer delay times. Initial radial velocity of ~100 m/s was reported by Zhang and Chait [18]. Taking into account the initial axial velocity (v_0= 850 m/s with 2,5 DHB matrix, see below) and the diameter of the aperture at the end of the second stage (2 mm), ions would be detected for delay time up to 10 μs. This supports the important role of the repulsive potential.

In the delay time range in which the ion time-of-flight changes linearly with t_d, the mean axial velocity was determined according to the model developed by Juhasz et al. [15]. This model assumes that: (1) ions are formed at the surface and (2) there is no residual electric in the first stage prior the ion extraction step. The ion time-of-flight linearly varies with the delay time. The slope is proportional to the initial velocity v_0, to a coefficient (depending upon d_1, d_2, L and G) and finally to $(m/2zeU)^{1/2}$. For each peptide ion, we verified that the experimental slopes (linear region) do not vary with G and U as expected by this model. The disagreement between the experimental results and the calculations is important especially for the light ions (matrix and substance P). A better agreement is only obtained for the insulin ions and from the experimental slopes, the initial axial velocity can be estimated to ~750 m/s. Moreover, the delay time for the maximum of resolution expected from this model remains still lower than that experimentally obtained, except for insulin and high G values (i.e. G=0.96). All these results turn out that in our experimental conditions, the residual electric field is non negligible and/or ions are not formed at the target surface.

The initial velocity previously determined for insulin, allows to estimate the ion initial kinetic energy, 0.45, 3.9, 7.8, 10.7, and 16.7 eV for 2,5-DHB, substance P, ACTH 18-39, ACTH 7-38 and insulin respectively. A direct comparison of these kinetic energies to the repulsing potential distribution highlights that, for the largest values of the delay time, ions come back to the target surface and no ion would

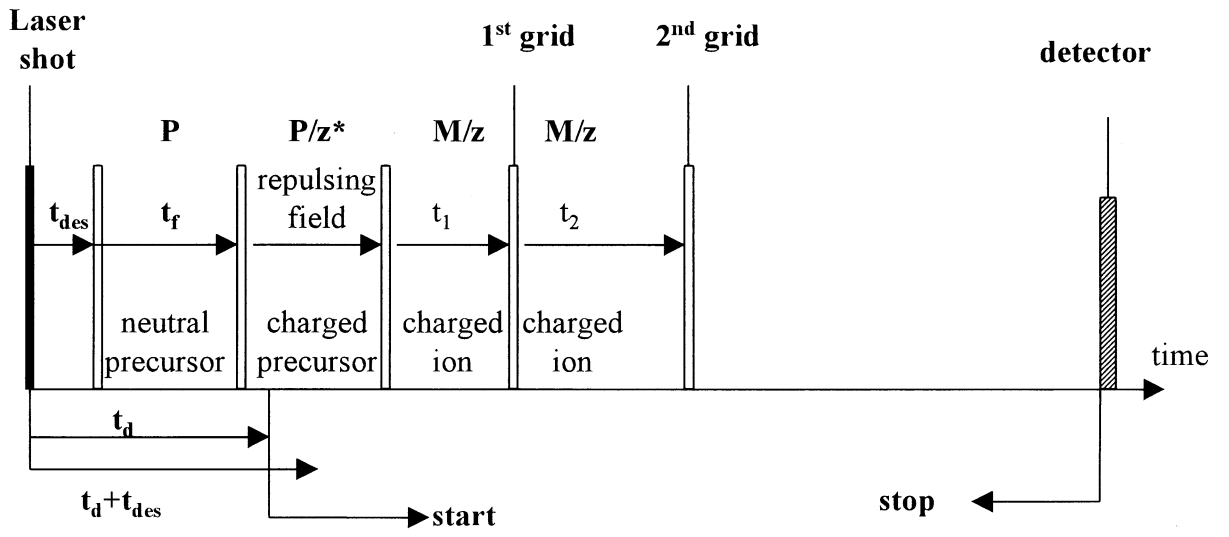

Fig. 5. Temporal scheme of the different events to calculate the ion flight time as a function of the delay time (see details in the text).

be detected. Typically, the calculated time needed for the return to the surface would be 69, 576, and 2 028 ns respectively for 2,5-DHB, substance P and insulin quasimolecular ions (U=20 kV and G=0.94). These time values are very short compared to the delay time range in which ions are detected, typically 1 100 ns for the 2,5 DHB ion. It turns out that ions are not formed on the surface but they originate from precursor species much more insensitive to the repulsing electric field. These precursors can be either neutral or charged with a much higher *m/z* ratio.

4. Discussion

The hypothesis of neutrals or charged precursors for the ion formation was checked by developing models from which the time-of-flight was calculated as a function of the delay time and the different parameters (ion *m/z*, G and U) and compared to the measured value.

In the delay time range (200–400 ns), the experimental ion time-of-flight was found to be roughly constant with respect to t_d for all the peptide ions. This suggests that in this time range, the ion precursor is rather insensitive to the repulsing field. Therefore, the precursor can be assumed to be neutral or with a high *m/z* ratio. The screening of the repulsing field by the high charge density near the surface cannot be ruled out [22], but its effect would be the same for all the ions. For higher values of the delay time, the precursor is charged and it is gradually decelerated (the deceleration varies as –z*eE/P for a precursor with a mass P and a charge z*e). Obviously, the precursor would be a noncovalent cluster composed by association of matrix molecules and analyte molecules. The relative low concentration of analyte in these experiments suggests that a peptide cluster-precursor contains at most one peptide molecule and likely the most abundant clusters are formed by matrix molecules only.

As ions are detected at their right *m/z* ratio, they are mainly accelerated with their own *m/z* ratio and thus, their precursors do not exist after the extraction pulse. This indicates that the complete desolvation of the charged precursor (ion stripping) would be triggered by the extraction pulse. The strong electric field variation during the pulse involves strong deceleration-acceleration forces promoting the separation between the charged ion and the noncovalent attached molecules in the precursor.

From these different outlines, a general model was developed. The scheme in Fig. 5, resumes the possible temporal sequence of the various events from the material ablation to the ion detection. This scheme takes into account: (1) a desorption time t_{des} i.e. the delay time between the laser shot and the ablation start, (2) a precursor ion formation time t_f corresponding to the time of the charge appearance on the precursor (mass P and charge z*e) after the ablation start, (3) up to the delay extraction time the precursor is decelerated in the repulsing field, and (4) at the extraction pulse time (t_d), the real ion appears (mass M and charge ze) and from its initial position and velocity it is accelerated in the extraction stages and finally detected after flying in the drift tube.

3.1. First model: constant repulsing field before extraction step

We first developed a simple model by considering a constant repulsing field Er ($Er=\alpha*G*U/d_1$). Time-of-flight calculations were performed by developing a program in Visual Basic (V5.0), involving the ion isotopic distribution and a initial axial velocity Gaussian distribution (100 velocity values were considered). This program allows to determine for the external parameter (ion *m/z* with z=1, G and U) the ion time-of-flight (peak centroid and FWHM, the percentage of detected ions) as a function of the delay time t_d. The percentage of detected ions corresponds to the number of ions, which were accelerated before reaching the target surface. A good agreement with the experimental results was found for the parameter values: $\alpha=0.0008$, $v_0=850$ m/s, $t_{des}=0$ ns and $t_f=300$ ns. In particular, these adjustments allows to predict correctly the t_d values for the matrix ion disappearance (due to its come back to the surface) and the maximum mass resolution. It should be noted that the repulsing field found in these simulations is roughly one order of magnitude lower than that estimated by SIMION ($\alpha\sim0.008$). Thus, the mass P of the ion precursor, before extraction, would also be one order of magnitude higher than the mass of the ion.

3.2. Second model: realistic repulsing field before the ion extraction step

A second model was developed taking into account the repulsing potential distribution depicted by SIMION. The ion time-of-flight was calculated (Visual Basic, V5.0) according to the ion motion in the temporal scheme given in Fig. 5. Before ion extraction i.e. for $t_f < t < t_d$, the ion precursor experiences the repulsing field and its motion was calculated by time steps of 1 ns. For the sake of simplicity, the natural isotopic distribution is not taken into account and only the time-of-flight was calculated for the chemical mass of the ion. The parameters (P, t_{des}, t_f, and v_0), giving the best agreement with experimental results (linear and non linear regions), are: $t_{des}<50$ ns, $t_f=300$ ns, and $v_0=850$ m/s. The mass of the ion precursor depends upon the mass of the analyte. For substance P, ACTH18-39, ACTH 7-38, bovine insulin and 2,5 DHB, the precursor mass range would be 10 000-15 000, 15 000–20 000, 15 000–30 000, 20 000–40 000, and 2 800–3 000 u, respectively. Fig. 6 compares the experimental results and the simulations for different precursor molecular weights respectively for substance P and bovine insulin. It must be noted that the agreement between experiments and simulations is better for G=0.90 (Fig. 6a and 6c) than for G=0.96 (Fig. 6b and 6d). In addition the delay time corresponding to the maximum resolution, assuming different initial velocities, was in better agreement with the experimental data for the different parameters (i.e. *m/z*, U and G).

We must outline that the different adjusted parameters do not play the same role and it is difficult to imagine that compensation effect occurs in the entire range of external parameters (*m/z*, G and U). The noncovalent precursor molecular weight estimated in this study may also originate from previous higher molecular weight precursors since during the dead time for ion extraction (~200 ns), natural desolvation can occur. In addition, the molecular weight of the precursor was determined for a unit charge and if the multiple charged precursors are considered, the real molecular weights have to be multiplied by the number of charges.

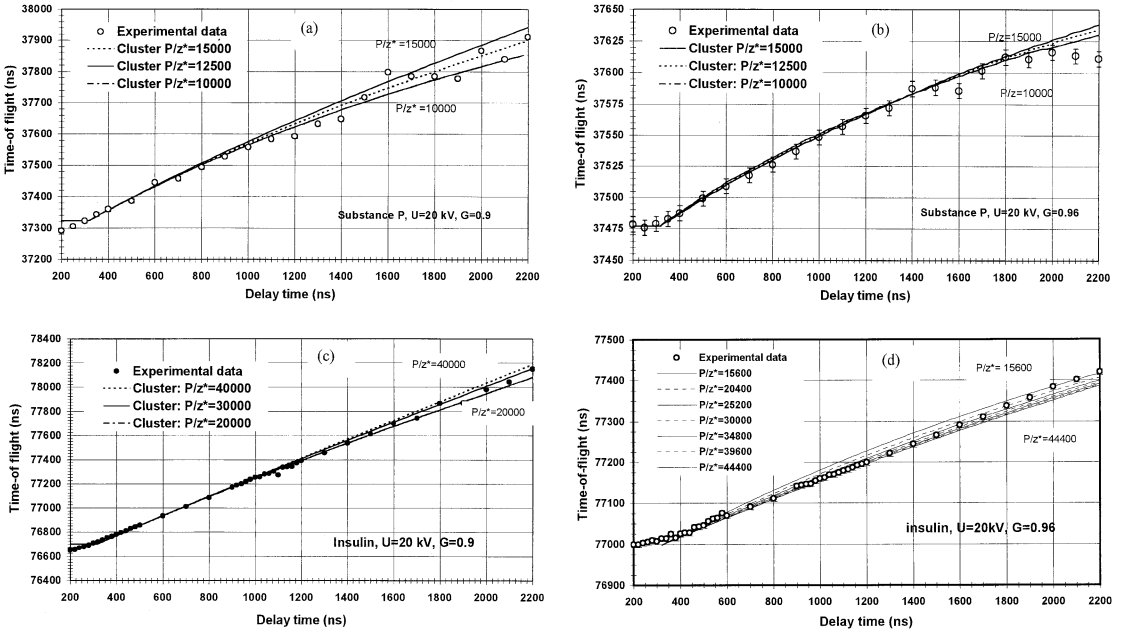

Fig. 6. Comparison of the experimental quasimolecular ion flight times (U=20 kV) and calculated values deduced from the second model for different cluster ion precursor P/z: (a) substance P and G=0.9, (b) substance P and G=0.96, (c) insulin and G=0.9 and (d) insulin and G=0.96. Note: in (a) and (b) the experimental flight times were increased by 10 ns and in (c) and (d) they were increased by 20 ns.

The fit, over the entire delay time range (~1 500–3 200 ns), requires to take into account a decreasing cluster molecular weight (z=1) with an increasing delay time especially for G=0.96 (high repulsing field). Typically for insulin, the cluster molecular weight 30 000 u fits correctly the low and medium t_d range and Mw= 20 000 u fits more correctly the t_d range higher than 1 800 ns (Fig. 6d) up to 3 200 ns (not shown). This can give evidence of natural desolvation of the cluster-precursor before ion extraction. Of course, a more complete description would need to take into account a distribution of precursors as well as their natural desolvation.

From these results, it was not possible to deduce a desorption time, t_{des}, as previously defined. We can only assume that this time would be extremely short (t_{de}< 50 ns). The time corresponding to the charge appearance on the precursor t_f = 300 ns and the initial velocity v_0= 850 m/s, are in good agreement with the value estimated from the first simple model. The initial axial velocity found in these simulations lies in the medium range of those determined by different methods [11–16]. One must note that the ion precursor and the presence of a repulsing electric field affect very smoothly the tof variation *vs.* t_d. Thus, if a limited number of delay times is considered, the determination of the initial velocity in delayed extraction can be underestimated in the case of a repulsing electric field.

As previously depicted, the molecular weight of the precursor ion (unity charge state) increases with the analyte molecular weight (size). Fig. 7 shows that a linear relationship can be established between the mean precursor molecular weight determined in these simulations and the power (2/3) of the analyte molecular weights. This relationship would suggest that if the analyte conformation is a sphere, the matrix molecules will be adsorbed on the surface of this sphere.

The cluster ejection in MALDI is not surprising and the recent molecular dynamics simulations by Zhigilei and Garrison [9] showed that droplet ejection is expected to occur in the ablation regime. These simulations do not strictly correspond to our experi-

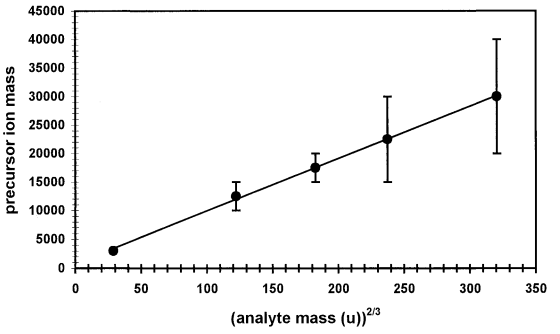

Fig. 7. Precursor ion molecular weight deduced from the second model (see text) as a function of the power 2/3 of the analyte molecular weight.

mental conditions since the laser pulse duration is much shorter (15 and 150 ps) than the classical N_2 laser (3 ns). However, the evolution of the ejected material as seen by these simulations is very useful to imagine what happens at the time scale of ns.

The natural desolvation of the cluster-precursor ion can explain some results on the axial and radial velocity. Due to the molecular weight difference between the analyte and matrix molecules, progressive desolvation of the cluster leads to a large scattering of low mass matrix molecules and a very low scattering of the analyte which continues in the initial direction of the cluster. This can explain the higher forward peaking of the analyte compared to matrix as experimentally observed on the radial velocity distribution [18] and expected from molecular dynamics simulations [9,23].

From the chemistry of the ion formation in MALDI, the role of cluster-precursor allows to draw a new frame. The idea that clusters are involved in the ionization processes induced by particle bombardment is not very new. Schmidt and Jungclas [24,25] have already suggested such a process (cluster born ions) in ^{252}Cf- PDMS. Recently, the model developed by Karas et al. [20] to account for the major phenomena in MALDI starts from the cluster ejection hypothesis and introduced a neutralization of the highest charge state by electrons to explain that the most abundant ion has a low charge state, mainly one, in MALDI. Experiments using delayed extraction also pointed out that analyte ionization (cationization and protonation) can be observed in the gas phase [26].

From our data, a strong difference appears between the precursors of the matrix and the analyte ions: the charges on the matrix precursor ion are already present 200 ns after the laser shot, when they appear 400 ns on the peptide containing precursor. As mentioned above, the extraction pulse promotes the stripping of the cluster and allows the sampling of the precursor ion composition. For matrix ions, the intensity increase in the t_d range (200–800 ns) suggests that the cluster charge increases with increasing time. Thus, electron(s) in the precursors must escape from the cluster with a probability increasing with time. It should be noted that the come back of non-neutralized electrons to the surface, accelerated by the attracting field, can be a major source of noise in the mass spectrum. In principle, the number of protonated matrix molecules must increase with t_d up to a plateau (escape of all electrons), but the repulsing field eliminate them progressively (Fig. 4c).

The increase of the peptide quasimolecular abundance for $t_d > 1\,000$ ns indicates that the proton transfer to analyte increases with time. As the size of the precursor decreases with time (natural desolvation) we can conclude that the proton transfer occurs preferentially when a peculiar size of the aggregates is achieved, for which the proton affinity of the matrix cluster becomes close to that of the peptide. In the delay time range of 200–400 ns, the precursors have no global charge. However, peptide quasimolecular are observed with a low abundance. This indicates that the proton transfer is already efficient involving likely the ejection of small size precursors.

From the discussion, a general scheme can resume the different steps leading to the formation of the analyte quasimolecular ion (Fig. 8). The chemical foundation of this simplified description will be discussed in the second part of this study [27], reporting similar study on the matrix α-cyano-4-hydroxycinnamic acid, in which thermochemical and kinetical considerations will be used to present an ionization model consistent with those occurring under IR-MALDI and electrospray conditions.

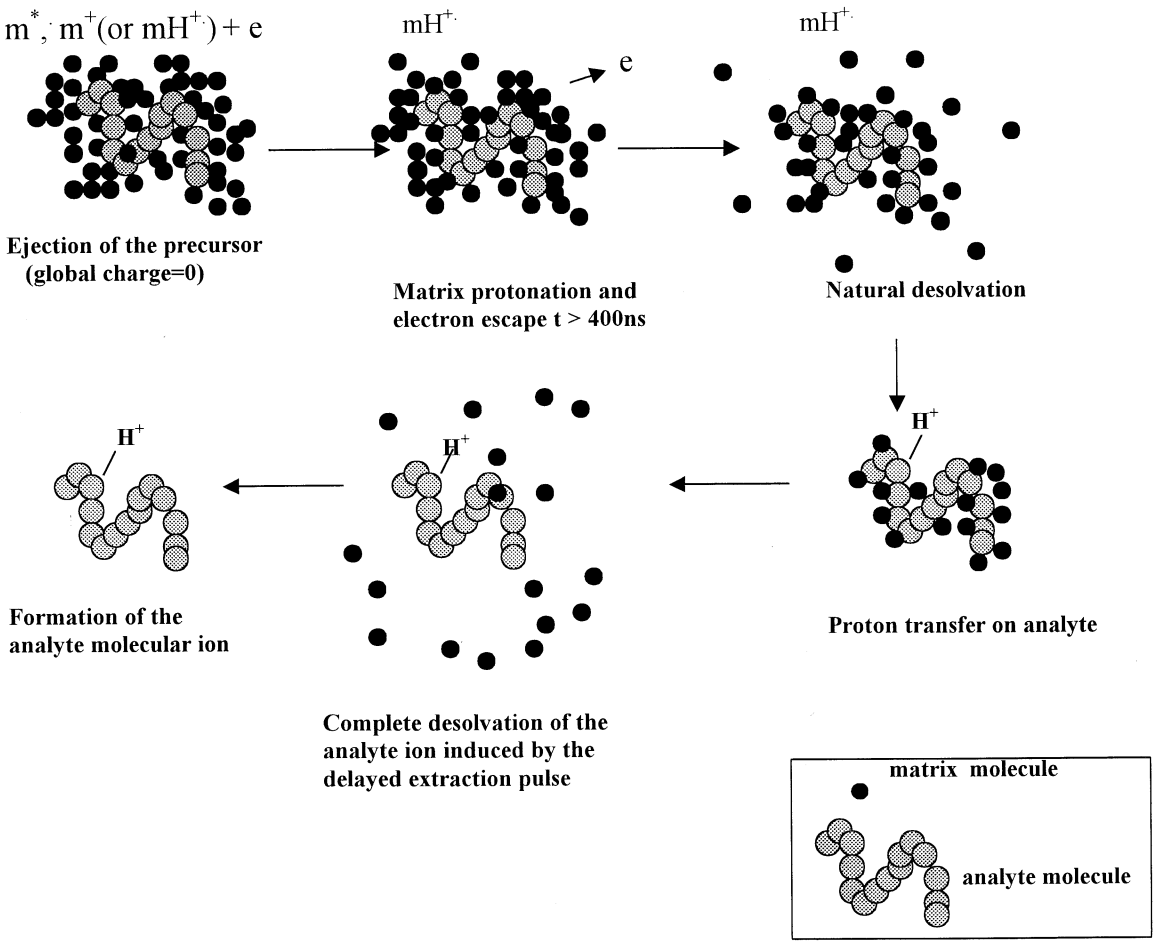

Fig. 8. A possible scenario for the formation of the analyte protonated molecule.

4. Conclusions

Matrix (2,5-DHB) and analyte molecular ion time-of-flight evolution and intensity as a function of the extraction delay time (200–2 200 ns) were carefully examined when a repulsing electric field is applied before the ion extraction step. The results clearly show that ions are not directly produced on the target but originate from higher mass precursors. A model based upon a cluster as ion precursor was developed to account for the effects experimentally observed. The model involved the cluster-precursor (P/z*), its motion in the repulsing field and a complete desolvation stimulated by the extraction pulse. The main result is that the precursor size increases with the molecular weight of analyte.

To go further in this dynamics study, the repulsing field must be more precisely adjusted through variation of distance and voltages in the first stage of the extraction region and the role of a low attracting field must also be explored. The ion precursor desolvation through the very fast voltage transient has also to be studied in detail. Similar studies in the delay time range below 200 ns would be very useful for a better understanding of the nature of the ion precursor and the role of natural desolvation. Such a methodology appears also to be very useful to draw a possible scenario of the analyte ion formation and to check the

associated chemical models in MALDI. Finally, these results highlight some common mechanisms with electrospray, from which ions are also formed from a condensed phase and followed by desolvation steps.

References

[1] W.V. Ligon, S.B. Dorn, Int. J. Mass Spectrom. Ion Processes 78 (1986) 99.
[2] H. Ehring, B.U.R. Sundqvist, J. Mass Spectrom. 30 (1995) 1303.
[3] H.C. Lüdemann, R.W. Redmond, F. Hillenkamp, Proceedings of the 48th ASMS Conference on Mass Spectrometry and Allied Topics (2000) 914.
[4] V. Karbach, R. Knochenmuss, Rapid Commmun. Mass Spectrom. 12 (1998) 968.
[5] D.A. Allwood, P.E. Dyer, R.W. Dreyfus, Rapid Commmun. Mass Spectrom. 11 (1997) 499.
[6] X. Tang, M. Sadeghi, Z. Olumee, A. Vertes, Rapid Commun. Mass Spectrom 11 (1997) 484.
[7] R. Knockenmuss, A. Vertes, J. Phys. Chem. B 104 (2000) 5406.
[8] L. Balazs, R. Gijbels, A. Vertes, Anal. Chem. 63 (1991) 314.
[9] L. V. Zhigilei, B. J. Garrison, J. Appl. Phys. 88 (2000) 1281.
[10] A.A. Puretzky, D.B. Geohegan, Appl. Surf. Sci. 127–129 (1998) 248.
[11] B. Spengler, R.J. Cotter, Anal. Chem. 62 (1990) 793.
[12] R C. Beavis, B.T. Chait, Chem. Phys. Lett. 181 (1991) 479.
[13] T. Huth-Fehre, C. H. Becker, Rapid Commun. Mass Spectrom. 5 (1991) 378.
[14] J. Zhou, W. Ens, K.G. Standing, A. Verentchikov, Rapid Commun. Mass Spectrom. 6 (1992) 671.
[15] P. Juhasz, M.L. Vestal, S.A. Martin, J. Am. Soc. Mass Spectrom. 8 (1997) 209.
[16] M. Glückmann, M. Karas, J. Mass Spectrom. 34 (1999) 467.
[17] W.Ens, Y. Mao, F. Mayer, K.G. Standing, Rapid Commun. Mass Spectrom. 5 (1991) 671.
[18] W. Zhang, B.T. Chait, Int. J. Mass Spectrom. Ion Processes 160 (1997) 259.
[19] R.Zenobi, R. Knockenmuss, Mass Spectrom.Rev. 17 (1998) 337.
[20] M. Karas, M. Glückmann, J. Schäeffer, J. Mass Spectrom. 35 (2000) 1.
[21] D.A. Dahl, SIMION 3D v6.0T Software, 43ed ASMS Conference (1995), 717.
[22] V. Bökelmann, B. Spengler, R. Kaufmann, Eur. J. Mass Spectrom. 1 (1995) 81.
[23] L.V. Zhigilei, B.J. Garrison, J. Appl. Phys. 71 (1997) 551.
[24] L. Schmidt, H. Jungclas, in “PDMS and clusters”, E.R. Hilf, F. Krammer, K. Wien (eds), Springer Lecture Notes in Physics, 269 (1987) 234.
[25] L. Schmidt, H. Jungclas: in “Ion Formation from Organics Solids (IFOS IV)”, A. Benninghoven (Ed.), Wiley, New York, 1989, p. 91.
[26] D.H. Wang, C. Dreisewerd, U. Bahr, M. Karas, F. Hillenkamp, J. Am. Soc. Mass Spectrom. 4 (1993) 393.
[27] I. Fournier, A. Brunot, J.C. Tabet, G. Bolbach (unpublished).